# Bifurcation to multisoliton complexes in the ac-driven, damped nonlinear Schrödinger equation

I. V. Barashenkov,* Yu. S. Smirnov,† and N. V. Alexeeva‡
*Department of Applied Mathematics, University of Cape Town, Private Bag Rondebosch 7700, South Africa*
(Received 22 May 1997)

We study bifurcations of localized stationary solutions of the externally driven, damped nonlinear Schrödinger equation $i\Psi_t+\Psi_{xx}+2|\Psi|^2\Psi=-i\gamma\Psi-he^{i\Omega t}$ in the region of large $\gamma$ ($\gamma>1/2$). For each pair of $h$ and $\gamma$, there are two coexisting solitons $\Psi_+$ and $\Psi_-$. As the driver's strength $h$ increases for the fixed $\gamma$, the $\Psi_+$ soliton merges with the flat background while the $\Psi_-$ forms a stationary collective state with two ''$\Psi$ pluses'': $\Psi_-\to\Psi_{(+-+)}$. We obtain other stationary solutions and identify them as multisoliton complexes $\Psi_{(++)},\Psi_{(--)},\Psi_{(-+)},\Psi_{(---)},\Psi_{(-+-)}$, etc. [S1063-651X(98)06002-4]

PACS number(s): 03.40.Kf, 05.45.+b, 75.30.Ds

## I. INTRODUCTION

### A. Motivation and outline

The present work deals with stationary localized solutions of the ac-driven, damped nonlinear Schrödinger (NLS) equation:

$$i\Psi_t+\Psi_{xx}+2|\Psi|^2\Psi=-i\gamma\Psi-he^{i\Omega t}. \tag{1}$$

Originally proposed as an amplitude equation for small-amplitude breathers in charge-density-wave materials in the presence of an applied ac field [1], this equation reappeared later in a variety of contexts. Among these are breathers in long Josephson junctions [2] and in easy-axis ferromagnets in a rotating magnetic field [3], as well as solitons in the rf-driven plasma [4,5]. More recently, Eq. (1) was used to describe temporal and spatial soliton propagation in a single-mode fiber ring cavity in the presence of an input forcing beam [6].

It was suggested by a simple two-particle variational argument that solitons of Eq. (1) may bind together to form bound states [7,8]. Independently, a similar prediction was made on the basis of the adiabatic equations of the inverse-scattering-based perturbation theory [9]. Subsequently, bound solitons were observed in direct numerical simulations of the full time-dependent NLS equation (1) [9,8]. However, although providing important insight when it is applicable, the perturbation theory cannot be used beyond small $h$ and $\gamma$. The applicability of the collective coordinate approach to the soliton dynamics is not unquestionable either. One of its drawbacks is that it can only be utilized for widely separated solitons; the other one is that it completely disregards radiation. (Skipping ahead a bit, it is fitting to note that results of the present work are not always in agreement with the collective coordinate predictions.) Furthermore, the variational approximation can be expected to be close to the actual solution only in the sense of the space-time average. In particular, one would not be able to use the variational method to draw a definite conclusion on the existence of *stationary* bound states. What the two-particle approximation would present as a time-independent bound state could in fact correspond to an oscillating association of two solitons with an infinite or finite lifetime.

The aim of the present work is to establish the existence of bound states without resorting to any kind of perturbative or variational arguments. (Consequently, we are not assuming the smallness of $h$ and $\gamma$.) We concentrate on *stationary* bound states; we expect that these will serve as a backbone for future analysis of oscillating and/or finite-lifetime soliton associations. Since for $\gamma\neq 0$ the system (1) is not conservative, it is not obvious how one could define the binding energy in this case. For this reason we avoid using the term ''bound state'' in what follows and refer to these objects as ''collective states,'' ''multisoliton complexes,'' or simply ''multisoliton solutions.'' By doing so we are also suggesting that the multisoliton complexes are not necessarily stable, a property that would be imperative for bound states. In addition to two-soliton complexes, we consider three-soliton collective states that appear to be equally fundamental from the bifurcation viewpoint. In what follows we study a variety of soliton associations: $\Psi_-$ with $\Psi_-$ (we denote this complex $\Psi_{(--)}$); $\Psi_+$ with $\Psi_+$ (to be denoted $\Psi_{(++)}$); $\Psi_{(-+)}$, $\Psi_{(+-+)}$, $\Psi_{(---)}$, $\Psi_{(-+-)}$, $\Psi_{(+++)}$, etc.

This paper has grown out of our attempts to tie up several loose ends left in our previous publication [10]. Those open problems concerned the domain of existence of the $\Psi_-$ soliton for large $\gamma$ ($\gamma>1/2$). Consequently, in the present work we concentrate on the case of *strongly* damped equations. In turn, our present findings indicate that the bifurcation diagram for *small* $\gamma$ can prove to be more complicated than it was originally thought in Ref. [10]. We are planning to return to the case of the weak damping in the future.

The paper is organized as follows. The next two subsections contain some technical preliminaries: In Sec. I B we give explicit formulas for the background flat-locked solution and in Sec. I C introduce the bifurcation measure that will be used throughout the paper. Section II is devoted to the bifurcation of the $\Psi_-$ soliton in the case of the strong damping ($\gamma>1/2$), the problem carried over from the previous paper [10]. We report a phenomenon not observed for $\gamma<1/2$: Instead of approaching an algebraic soliton as in the

*Electronic address: igor@uctvms.uct.ac.za
†Present address: Joint Institute for Nuclear Research, LCTA, Dubna 141980, Russia.
Electronic address: smirnov@maths.uct.ac.za
‡Electronic address: nora@maths.uct.ac.za

 © 1998 The American Physical Society

case of the weak damping, the $\Psi_-$ turns into a new branch of three-soliton solutions. This branch appears to be not unique; a host of other localized solutions is presented in Sec. IV. These results are preceded (Sec. III) by the description of a variational formalism (a generalization of the one employed in [7,8]), which we then use to identify different localized solutions as two- and three-soliton complexes. (Thus the variational formalism plays only an auxiliary role in this work.) Our key result is the bifurcation diagram (Fig. 5) illustrating links and relationships between all soliton complexes obtained so far. Finally, in Sec. V several concluding remarks are made.

### B. Flat background

As in [10] we fix, without loss of generality, $\Omega=1$ and perform the transformation $\Psi(x,t)=e^{it}\psi(x,t)$, reducing Eq. (1) to an autonomous equation

$$i\psi_t+\psi_{xx}-\psi+2|\psi|^2\psi=-i\gamma\psi-h. \tag{2}$$

The advantage is that we will be able to deal with time-independent solutions instead of periodic ones. The time-independent solutions of Eq. (2) satisfy

$$\psi_{xx}-\psi+2|\psi|^2\psi=-i\gamma\psi-h; \tag{3}$$

this is the equation that we are going to study in this paper. We first recall briefly some facts about the *flat-locked* (or continuous-wave) solutions to Eq. (1), i.e., $x$-independent solutions of Eq. (3). It is convenient to decompose $\psi_0$ as $\psi_0=\sqrt{\rho_0}\exp(i\theta)$; then

$$\tan\theta=\frac{\gamma}{1-2\rho_0},\quad 0\leqslant\theta\leqslant\pi,$$

and $\rho_0$ is a root of the cubic equation

$$4\rho_0^3-4\rho_0^2+(1+\gamma^2)\rho_0-h^2=0. \tag{4}$$

Approximate [5,11] and numerical [12] solutions of Eq. (4) are available for small $h$ and $\gamma$. The analysis for general $h$ and $\gamma$ is presented in our previous publication [10]. Although we did not write out explicit formulas for the roots, we identified regions of characteristic behavior of the roots on the $(h,\gamma)$ plane and gave analytic expressions for boundaries between these regions. In fact, explicit roots can be easily found; we list them here and will utilize them in subsequent calculations.

An explicit formula for the roots is written in terms of coefficients of the associated incomplete cubic equation

$$y^3+Py+Q=0,$$

where $y=\rho_0-1/3$ and the coefficients are given by

$$P=\frac{1}{4}\left(\gamma^2-\frac{1}{3}\right)$$

and

$$Q=\frac{1}{12}\left(\gamma^2+\frac{1}{9}-3h^2\right).$$

The number of real (positive) roots varies with $h$ and $\gamma$. Two characteristic regions of $\gamma$ can be identified as follows.

*First*, when $\gamma\leqslant 1/\sqrt{3}$, the coefficient $P$ is negative and Eq. (4) may have one or three real positive roots, depending on how $h$ compares with $h_+$ and $h_-$, where

$$h_\pm=h_\pm(\gamma)=\left\{\frac{1}{3}\left(\gamma^2+\frac{1}{9}\right)\pm\frac{1}{3}\sqrt{\frac{1}{3}\left(\frac{1}{3}-\gamma^2\right)^3}\right\}^{1/2}. \tag{5}$$

If $h$ is greater than $h_+$ or smaller than $h_-$, the discriminant of Eq. (4),

$$\mathcal{D}=-108\left\{\left(\frac{P}{3}\right)^3+\left(\frac{Q}{2}\right)^2\right\}, \tag{6}$$

is negative and the equation has only one real root

$$\rho_0=\frac{1}{3}-2\left(-\frac{P}{3}\right)^{1/2}\frac{1}{\sin(2\alpha)},$$

where

$$\tan\alpha=\left(\tan\frac{\beta}{2}\right)^{1/3}\quad\left(|\alpha|\leqslant\frac{\pi}{4}\right)$$

and

$$\sin\beta=\frac{2}{Q}\left(-\frac{P}{3}\right)^{3/2}\quad\left(|\beta|\leqslant\frac{\pi}{2}\right).$$

Here positive values of $Q$, $\alpha$, and $\beta$ correspond to $h<h_-$ and

$$\rho_0<\frac{1}{3}-\frac{1}{3}\sqrt{1-3\gamma^2}.$$

Negative $Q$, $\alpha$, and $\beta$ pertain to $h>h_+$ and

$$\rho_0>\frac{1}{3}+\frac{1}{3}\sqrt{1-3\gamma^2}.$$

If $\gamma\leqslant 1/\sqrt{3}$ and $h$ falls between $h_-$ and $h_+$, the discriminant (6) is positive and there are three positive roots $0<\rho_0^{(1)}<\rho_0^{(2)}<\rho_0^{(3)}$:

$$\rho_0^{(j)}=\frac{1}{3}-2\left(-\frac{P}{3}\right)^{1/2}\cos\left[\frac{\alpha}{3}+(-1)^j\frac{\pi}{3}\right],\quad j=1,2$$

$$\rho_0^{(3)}=\frac{1}{3}+2\left(-\frac{P}{3}\right)^{1/2}\cos\left(\frac{\alpha}{3}\right),$$

where

$$\cos\alpha=-\frac{Q/2}{(-P/3)^{3/2}}\quad(0\leqslant\alpha\leqslant\pi).$$

It is not difficult to find the ranges of the above roots:

$$\frac{1}{3}-\frac{1}{3}\sqrt{1-3\gamma^2}\leqslant\rho_0^{(1)}\leqslant\rho_-(\gamma),$$

$$\rho_-(\gamma)\leqslant\rho_0^{(2)}\leqslant\rho_+(\gamma),$$

$$\rho_+(\gamma)\leqslant\rho_0^{(3)}\leqslant\frac{1}{3}+\frac{1}{3}\sqrt{1-3\gamma^2},$$

where

$$\rho_\pm(\gamma)=\frac{1}{3}\pm\frac{1}{6}\sqrt{1-3\gamma^2}. \tag{7}$$

In the *second* region defined by $\gamma\geqslant 1/\sqrt{3}$, the coefficient $P$ is positive, discriminant negative, and we only have one real (positive) root

$$\rho_0=\frac{1}{3}-2\left(\frac{P}{3}\right)^{1/2}\cot(2\alpha),$$

where

$$\tan\alpha=\left(\tan\frac{\beta}{2}\right)^{1/3}\quad\left(|\alpha|\leqslant\frac{\pi}{4}\right)$$

and

$$\tan\beta=\frac{2}{Q}\left(\frac{P}{3}\right)^{3/2}\quad\left(|\beta|\leqslant\frac{\pi}{2}\right).$$

This completes the description of the flat solutions of Eq. (3).

### C. Bifurcation measure

In order to describe transformations and bifurcations of solutions to Eq. (3) quantitatively, we need a real-valued functional that would represent solutions as points in $\mathbb{R}^1$. In our previous publication [10] we used the value $|\psi(0)|^2$ as a bifurcation measure. The disadvantage of this measure is that it is very sensitive to numerically induced shifts of the solution as a whole: $\psi(x)\to\psi(x-x_0)$. Also, it completely disregards the variation of the soliton's shape away from the point $x=0$, while it is precisely the soliton's ''wings'' that change most significantly as new solitons attach to the multisoliton state. For these and some other reasons that will become clear below, we find it useful to replace the single-point measure by an integral characteristic of solutions.

Using Eq. (2), it is straightforward to verify that

$$\frac{dE}{dt}+2\gamma E=2\gamma\int\left\{|\psi|^4-\frac{h}{2}(\psi+\overline{\psi})-|\psi_0|^4+\frac{h}{2}(\psi_0+\overline{\psi_0})\right\}dx, \tag{8}$$

where

$$E=\int\{|\psi_x|^2+|\psi|^2-|\psi|^4-h(\psi+\overline{\psi})-|\psi_0|^2+|\psi_0|^4+h(\psi_0+\overline{\psi_0})\}dx. \tag{9}$$

When $\gamma=0$, the quantity $E$ is conserved and represents the energy of the system. In this case the energy is a natural and physically meaningful choice for the bifurcation measure. We have found it useful to retain $E$ [Eq. (9)] as a bifurcation measure even in the case $\gamma\neq 0$, when it is not conserved. Although the meaning of this quantity is not so obvious for nonsmall $\gamma$, we will still be referring to $E$ as energy. As opposed to $|\psi(0)|^2$, the measure $E$ is additive: When new solitons attach to the collective state, the energy of the complex will increase by the amount close to the energy of new constituents.

When $\psi$ is a time-independent solution, we have $dE/dt=0$ and Eq. (8) gives a useful representation for the energy of *static* solutions

$$E=\int\left\{|\psi|^4-\frac{h}{2}(\psi+\overline{\psi})-|\psi_0|^4+\frac{h}{2}(\psi_0+\overline{\psi_0})\right\}dx. \tag{10}$$

This formula is particularly efficient in numerical calculations as it does not involve derivatives of $\psi$.

## II. BIFURCATION OF THE $\psi_-$ SOLITON

We start with returning to a question that remained unanswered in our previous publication [10]. There, we attempted to find, numerically, the upper boundary of the domain of existence of the $\psi_+$ and $\psi_-$ solitons.

### A. Types of asymptotic decay

In order to find the upper boundary, it is useful to consider first the asymptotic region $|x|\to\infty$. The solitons decay to the value $\psi_0$ exponentially:

$$\psi_\pm(x)-\psi_0\sim e^{(-p+ik)|x|}\quad\text{as}\quad|x|\to\infty,$$

where $p,k>0$ and the complex exponent $\kappa=-p+ik$ satisfies

$$(\kappa^2)_{1,2}=1-4|\psi_0|^2\pm\sqrt{4|\psi_0|^4-\gamma^2}. \tag{11}$$

Both $(\kappa^2)_1$ and $(\kappa^2)_2$ are negative for certain $|\psi_0|^2$ and hence there can be no solitons with these asymptotic values. In the region $\gamma>1/\sqrt{3}$ this happens for $|\psi_0|^2>\gamma/2$; in the region $1/2<\gamma<1/\sqrt{3}$ both $\kappa^2$ are negative for $\gamma/2<|\psi_0|^2<\rho_-$ and for $|\psi_0|^2>\rho_+$; finally, in the region $\gamma<1/2$ this situation takes place for $|\psi_0|^2>\rho_+$. [Here $\rho_-$ and $\rho_+$ are as in Eq. (7).] Next, when $|\psi_0|^2$ lies between $\rho_-$ and $\rho_+$, one root $(\kappa^2)_1$ is positive and the other one $(\kappa^2)_2$ negative. There can, in principle, exist solutions with such asymptotic values. However, none were found [10]. Furthermore, flat solutions with $\rho_-<|\psi_0|^2<\rho_+$ are unstable [10] and hence these solitons would be of little interest even if they existed.

There are two ranges of $|\psi_0|^2$ where solitons were found. The first one is $|\psi_0|^2<\gamma/2$ (for all $\gamma$). Here both $(\kappa^2)_{1,2}$ are complex yielding nonzero $p$ and $k$. The solitons undergo an oscillatory decay to the flat background, with the decay rate

$$p=\left\{\frac{1-4|\psi_0^2|}{2}+\frac{\sqrt{(1-4|\psi_0|^2)^2+\gamma^2-4|\psi_0|^4}}{2}\right\}^{1/2} \tag{12}$$

and the wave number of undulations

$$k=\frac{\sqrt{\gamma^2-4|\psi_0|^4}}{2p}. \tag{13}$$

For $\gamma<1/2$ there is also another range $\gamma/2<|\psi_0|^2<\rho_-$. Here both $\kappa^2$ are positive and solitons approach their asymptotic values monotonically ($k=0$), with the decay exponent

$$p=\{1-4|\psi_0|^2-\sqrt{4|\psi_0|^4-\gamma^2}\}^{1/2}. \tag{14}$$

The inequality $|\psi_0|^2<\gamma/2$ can be rewritten as $h<h_*(\gamma)$, where

$$h_*(\gamma)\equiv(\gamma^3-\gamma^2+\gamma/2)^{1/2}, \tag{15}$$

and now we can summarize our conclusions in terms of $h$ and $\gamma$: For small $\gamma$, $\gamma<1/2$, the $\psi_+$ and $\psi_-$ solitons can only exist for $h<h_+$. They exhibit two types of asymptotic decay: monotonic for $h_*<h<h_+$ and oscillatory for $h<h_*$. The corresponding decay rates are given by Eqs. (14) and (12), respectively. On the contrary, in the region $\gamma>1/2$ the decay is always oscillatory. Here there can be no localized solutions above the value $h=h_*$. For $h<h_*$, the decay exponent is given by Eq. (12) and the wave number of the asymptotic undulations by Eq. (13).

### B. Weak damping ($\gamma<1/2$)

Now we are prepared to discuss soliton transformations in the vicinity of the upper boundary of their domain of existence. Assume $\gamma$ is smaller than 1/2 and fixed. As $h$ increases to the value $h_+$, where $h_+(\gamma)$ is given by Eq. (5), the decay exponent $p$ [Eq. (14)] goes to zero. The fate of the two solitons $\psi_+$ and $\psi_-$ turns out to be different.

The amplitude of the $\psi_+$ soliton was observed to decrease while its characteristic width was increasing and eventually the $\psi_+$ was seen to merge with the flat solution: $\psi_+(x)\to\psi_0$ as $h\uparrow h_+$. This numerical observation is in agreement with the asymptotic series representation of the soliton $\psi_+$ [13]. On the contrary, the soliton $\psi_-$ retained a finite amplitude and remained well localized in this limit (though the decay exponent $p$ did tend to zero). We were able to obtain this solution in a very near vicinity of the point $h_+$. [More precisely, we succeeded in finding the $\psi_-$ with the asymptotic value $|\psi_0|^2$ deviating not more than by $10^{-3}$ from the curve $\rho_-(\gamma)$. In terms of $h$, this means that the upper boundary is given by $h_+(\gamma)$ to within the accuracy of order $10^{-6}$.] This implies that as $h\to h_+$, the soliton $\psi_-$ tends to a localized solution decaying as a negative power of $x$. (There is a very subtle question of whether the $\psi_-$ exists *arbitrarily* close to $h_+$, i.e., whether this algebraic soliton is actually reached. We return to this issue in Sec. V.) The soliton transformation can be conveniently characterized by the variation of the energy with $h$; this is shown in Fig. 1.

### C. Strong damping ($\gamma\geq 1/2$)

The situation in the region $\gamma\geq 1/2$ turned out to be more complicated. In this region the decay rate is given by Eq. (12); as we mentioned in Sec. II A, it goes to zero as $h$

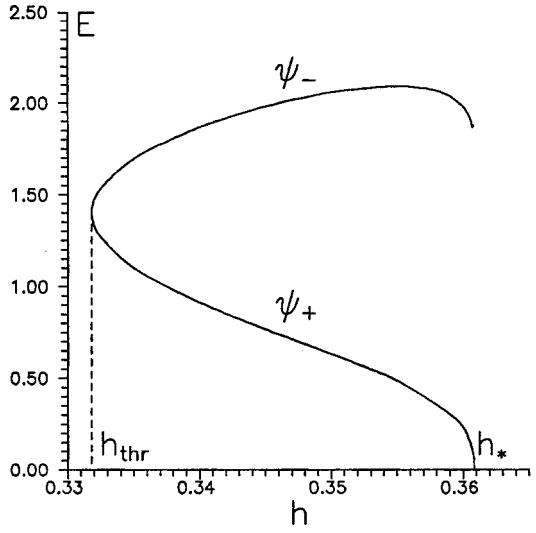


FIG. 1. Typical bifurcation diagram of the one-soliton solution. (In this picture $\gamma=0.52$.) At the point $h=h_*=0.360\,843$ (where $|\psi_0|^2=\gamma/2=0.26$) the soliton $\psi_+$ detaches from the flat solution (whose energy is zero.) The point $h_{\rm thr}=0.331\,806\,5$ is a turning point; at this point the $\psi_+$ soliton transforms into the $\psi_-$ solution. The $\psi_-$ soliton ceases to exist for $h>0.360\,792\,1$ or, equivalently, for $|\psi_0|^2>0.254\,416\,8$. It remained unclear in Ref. [10] what happens to the $\psi_-$ branch beyond that point. The diagram for the case $\gamma<1/2$ would look qualitatively similar; the only difference would be that in the latter case, the domains of existence of $\psi_+$ and $\psi_-$ coincide.

$\to h_*$ and $|\psi_0|^2\to\gamma/2$. Similarly to the case $\gamma<1/2$, the $\psi_+$ soliton was observed to merge with the flat solution here; see Fig. 1. (We were able to find the $\psi_+$ arbitrarily close to the value $h=h_*$.) It was natural to expect that the $\psi_-$ soliton would also behave as in the $\gamma<1/2$ case. As we have already mentioned, in the region $\gamma<1/2$ we succeeded in finding the $\psi_-$ soliton with the asymptotic value $|\psi_0|^2$ deviating from $\rho_-(\gamma)$ not more than by $10^{-3}$. On the contrary, when $\gamma>1/2$, the upper boundary of its domain of existence was found to deviate quite substantially from the curve $|\psi_0|^2=\gamma/2$. The question of what causes this deviation and what finally happens to the $\psi_-$ soliton as $h$ increases was left open in Ref. [10].

In order to clarify the situation, we have designed a sixth-order accurate numerical algorithm based on the continuous analog of Newton's method and performed a detailed study of the neighborhood of the point $h=h_*$. (For references and a brief review of the method, see [10].) Results of this study are presented in Figs. 2 and 3. This more accurate analysis has revealed that the reason why we were not able to approach the point $h=h_*$ close enough in Ref. [10] was the existence of a new turning point. At this point the $\psi_-$ branch turns into a new branch of localized solutions; see Fig. 3. Solutions of this branch are nonlinear superpositions of three solitons: the $\psi_-$ soliton in the middle and two $\psi_+$ solitons at its sides.

A more extensive search has led to a larger variety of multisoliton complexes. The corresponding energies are plotted in the bifurcation diagram (Fig. 5, Sec. IV). Before proceeding to the description of the diagram, we first need to

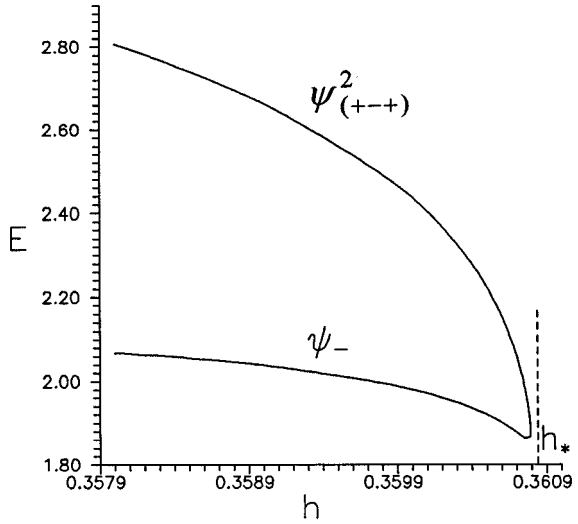


FIG. 2. Bifurcation to a three-soliton complex for $\gamma=0.52$. The lower branch here is the extreme right part of the $\psi_-$ branch from Fig. 1. The solution corresponding to the upper curve is plotted in Figs. 3(c) and 3(d).

introduce a simple variational formalism which will allow us to identify its various branches.

### III. COLLECTIVE COORDINATE DESCRIPTION

As we have already mentioned in the Introduction, one could not rely on the variational (or collective-coordinate) approach to demonstrate the existence of stationary multisoliton solutions. However, the variational description proves to be quite useful in the *a posteriori* identification of the numerically obtained soliton complexes.

It is convenient to consider three-soliton configurations first; the two-soliton state will be obtainable as a simple particular case. We set up a trial function in the form of a linear combination

$$\psi_1\psi_2\psi_3(x;z)\equiv\psi_1+\psi_2+\psi_3-2\psi_0, \tag{16}$$

where

$$\psi_1=\psi_1(x+z), \quad \psi_2=\psi_2(x), \quad \psi_3=\psi_3(x-z)$$

are three different or identical solitons sitting at the points $x=-z$,0, and $+z$, respectively. Here $z$ is a positive value that is allowed to depend on time: $z=z(t)$. We have to use a bit awkward notation $\psi_1\psi_2\psi_3$ in order to distinguish the *linear combination* of three solitons from the *genuine three-soliton solution*; our notation for the latter would be $\psi_{(123)}$.

The damped driven NLS equation (1) follows from the stationary action principle $\delta S=0$, where

$$S=\int e^{2\gamma t}L[\psi,\overline{\psi}]dt \tag{17}$$

and the Lagrangian $L=T-E$ comprises the kinetic

$$T=\frac{i}{2}\int_{-\infty}^{\infty}(\psi_t\overline{\psi}-\overline{\psi_t}\psi)dx \tag{18}$$

and ''potential'' term

$$E=\int_{-\infty}^{\infty}\{|\psi_x|^2+|\psi|^2-|\psi|^4-h(\psi+\overline{\psi})-|\psi_0|^2+|\psi_0|^4 +h(\psi_0+\overline{\psi_0})\}dx. \tag{19}$$

Substituting the ansatz (16) into Eqs. (18) and (19), we obtain for the kinetic term

$$T=T_{11}+T_{33}+T_{13}+T_{12}+T_{23}, \tag{20}$$

where

$$T_{11}=\frac{i}{2}\dot{z}\int\left\{\frac{d\psi_1}{dx}(\overline{\psi_1}-\overline{\psi_0})-\text{c.c.}\right\}dx, \tag{21}$$

$$T_{33}=-\frac{i}{2}\dot{z}\int\left\{\frac{d\psi_3}{dx}(\overline{\psi_3}-\overline{\psi_0})-\text{c.c.}\right\}dx, \tag{22}$$

$$T_{13}=\frac{i}{2}\dot{z}\int\left\{\left(\frac{d\psi_1}{dx}\overline{\psi_3}+\psi_1\frac{d\overline{\psi_3}}{dx}\right)-\text{c.c.}\right\}dx =\frac{i}{2}\dot{z}(\psi_1\overline{\psi_3}-\psi_3\overline{\psi_1})\Big|_{-\infty}^{+\infty}, \tag{23}$$

and

$$T_{12}+T_{23}=\frac{\dot{z}}{2}\frac{d\sigma}{dz},$$

with

$$\sigma(z)=i\int\{(\overline{\psi_2}-\overline{\psi_0})(\psi_1+\psi_3)-\text{c.c.}\}dx. \tag{24}$$

In the above formulas, $\psi_1=\psi_1(x+z)$, $\psi_2=\psi_2(x)$, and $\psi_3=\psi_3(x-z)$. The terms $T_{11}$ and $T_{33}$ vanish because $\psi_1(x)$ and $\psi_3(x)$ are even functions and $T_{13}=0$ because $\psi_1$ and $\psi_3$ approach the same value $\psi_0$ at plus and minus infinity.

We now have

$$L=\frac{\dot{z}}{2}\frac{d\sigma}{dz}-E(z),$$

where $E=E[\psi_1\psi_2\psi_3(x;z)]$ is the functional (19) evaluated at the linear combination (16). Varying the action (17) yields

$$\frac{d}{dz}(E+\gamma\sigma)\equiv\frac{dU_{\text{eff}}}{dz}=0. \tag{25}$$

Equation (25) is of the form of a constraint; it describes only stationary solutions. We could have easily made it dynamical just by adding one more time-dependent variable (the canonically conjugate momentum), but since we are only interested in stationary configurations, Eq. (25) is quite sufficient for our purposes.

In the three-soliton case, we confine ourselves to *symmetric* configurations and assume that $\psi_1(x)=\psi_3(x)$. In this case the ansatz (16) describes two identical solitons $\psi_1$ (which can be either two $\psi_+$'s or two $\psi_-$'s) placed at the distance $2z$ from one another and an additional soliton $\psi_2$ sitting symmetrically in between. The intermediate soliton

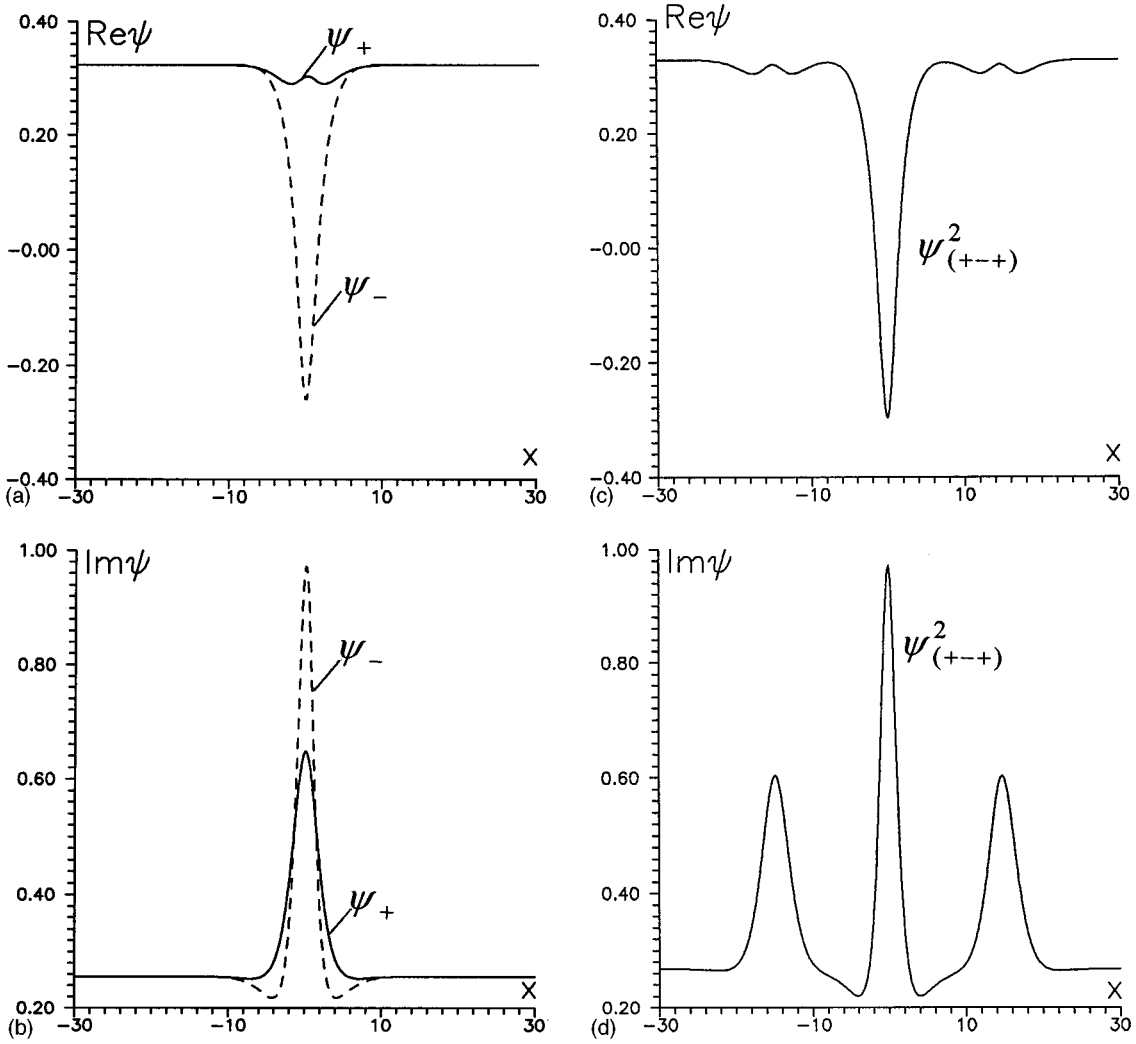


FIG. 3. Localized solutions corresponding to three branches of the bifurcation diagram in Figs. 1 and 2. Shown are the (a) real and (b) imaginary parts of $\psi_+$ (solid line) and $\psi_-$ (dashed line); these two solutions correspond to the lowest and middle branches, respectively. (c) and (d) New branches into which the $\psi_-$ solution turns at the point $h=0.360\,792\,1$. A comparison of (a) to (c) and (b) to (d) reveals that the last solution is a combination of one $\psi_-$ and two $\psi_+$ solitons. (Below we call this complex $\psi^2_{(+-+)}$.) In these pictures, $\gamma=0.52$ and $h=0.35$.

can be of the same variety as the two side ones (like in $\psi_{(+++)}$) or of a different kind (e.g., $\psi_{(+-+)}$). Notice that the function

$$\psi_1+\psi_3=\psi_1(x+z)+\psi_1(x-z)$$

is even and so the term $T_{12}+T_{23}$ does not necessarily have to be equal to zero.

The two-soliton case arises if we eliminate the middle soliton by setting $\psi_2(x)\equiv\psi_0$; then the quantity $\sigma$ vanishes. In this case we do not need to assume that $\psi_1(x)=\psi_3(x)$; $\psi_1$ and $\psi_3$ can stand for any combination of $\psi_+$ and $\psi_-$ solitons. The Euler-Lagrange equation (25) reduces simply to

$$\frac{dE}{dz}=0. \tag{26}$$

This is almost the same variational principle as the one employed in [7,8]. The only difference is that we are using the total energy (19), while the authors of [7,8] utilized only the interaction term $\int|\psi|^4dx$.

For small $h$ and $\gamma$ the solitons can be approximated by explicit formulas. In this case, assuming a wide separation between the two solitons, the integral (19) can be evaluated analytically [7,8] and Eq. (26) has a sequence of roots (''two-soliton orbits'') $z_n$:

$$2z_n=\frac{\pi}{2k}(2n-1),\quad n=1,2,3,\ldots, \tag{27}$$

where $k$ is the soliton's asymptotic wave number

$$\psi(x)-\psi_0\sim e^{(-p+ik)|x|}\quad\text{as}\quad|x|\to\infty.$$

Expression (27) applies uniformly to all three two-soliton linear combinations ($\psi_+\psi_+$, $\psi_-\psi_-$, and $\psi_-\psi_+$). Although Eq. (27) was derived for small $h$ and $\gamma$ only, the general argument behind this result is more general. It simply states that when two solitons are widely separated, the first soliton is only affected by the *tail* of the second one, and since the tails have undulations, the potential of interaction exhibits

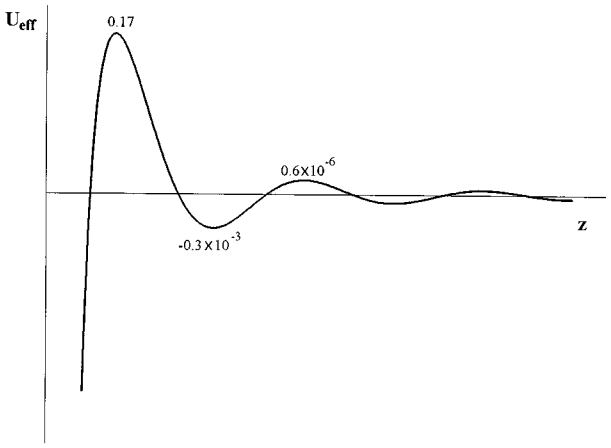


FIG. 4. Energy of the two-soliton linear combination $\psi_-\psi_- = \psi_-(x+z)+\psi_-(x-z)-\psi_0$ as a function of the intersoliton separation $2z$. The energies of the other two-soliton linear combinations $\psi_+\psi_+$ and $\psi_-\psi_+$ as well as of four symmetric three-soliton superpositions ($\psi_+\psi_+\psi_+$, $\psi_-\psi_-\psi_-$, $\psi_+\psi_-\psi_+$, and $\psi_-\psi_+\psi_-$) look qualitatively similar.

alternating minima and maxima [7,8]. Consequently, one can expect Eq. (27) with $k$ defined by Eqs. (12) and (13) to be applicable in a somewhat wider domain than just for very small $h$ and $\gamma$.

## IV. MULTISOLITON BIFURCATION DIAGRAM

Using the numerically precomputed solitons $\psi_-$ and $\psi_+$, we have evaluated the effective potential of interaction $U_{\text{eff}} = E+\gamma\sigma$ for all three two-soliton and all four symmetric three-soliton combinations. The potential is shown, as a function of the intersoliton separation $z$, in Fig. 4. This particular figure corresponds to the $\psi_-\psi_-$ linear combination; for all other two- and three-soliton combinations the potential looks qualitatively similar. The potential of the soliton-soliton interaction is attractive at short distances and then intervals of attraction and repulsion alternate. As in the preceding section, the consecutive points of extrema are denoted by $z_n$: $z_1$ is a maximum, $z_2$ minimum, and so on. A reservation that we have to make here is that it is only for sufficiently large intersoliton separations that the energy $U_{\text{eff}}$ of the above linear combinations yields the true potential of the soliton-soliton interaction.

The positions of the first three extrema obtained in this way are given in Tables I and II (second column). In the first column of this table we give the genuine values of the intersoliton separation, i.e., the separations exhibited by the numerical solutions of Eq. (3). (Notice that in the two-soliton case, the separation distance between the solitons is $2z$ not $z$.) Finally, the third column contains the separation distances as obtained by the approximate formula (27).

### A. Two-soliton complexes

Numerically, we were able to find *five* different two-soliton complexes: four symmetric and one asymmetric. The corresponding energies are shown in Fig. 5. It is convenient to start with two distinct two-$\psi_+$ soliton solutions that detach from the flat solution at $h=h_*$. For the driver's strength $h=0.35$ (which will be used as a reference value throughout the paper), the corresponding separations are $2z_1\approx 7.60$ and $2z_3\approx 28.00$. By comparing to the predictions of the variational analysis (which gives $2z_1=7.95$, $2z_2=18.20$, and $2z_3=28.45$; see Table I) one of these solutions can be identified with the first orbit (we denote it $\psi^1_{(++)}$) and the other with the *third*, to be denoted $\psi^3_{(++)}$ (hence the notation $z_1$ and $z_3$). Surprisingly, we were not able to find numerically the two-$\psi_-$ soliton complex with the solitons sitting at the *second* orbit $z_2$.

Both numerically found two-$\psi_+$ soliton solutions are shown in Fig. 6. In order to rule out any doubts about whether the $\psi^1_{(++)}$ solution is really an association of two ''$\psi$ pluses,'' we have also drawn, on the same set of axes, the linear combination $\psi_+(x+z)+\psi_+(x-z)-\psi_0$. Here we have taken $z=z_1$, where $z_1$ is equal to the *numerically observed* value of the separation (and not to the maximum of the corresponding two-soliton interaction potential). We do not plot the above linear combination for $z=z_3$ as it would be indistinguishable from the actual $\psi^3_{(++)}$.

As the driving strength $h$ is decreased down to $h_{\text{thr}}=0.331\,806\,5$ (which coincides with the threshold value for the one-soliton solution), the $\psi^3_{(++)}$ complex turns into the solution that can be interpreted as $\psi^3_{(--)}$. For our reference value of $h$, $h=0.35$, the intersoliton separation of this new complex is $2z_3\approx 26.20$, while the variational method gives $2z_3=25.60$.

The threshold driving strength (i.e., the lower boundary of the domain of existence) for the lowest orbit $\psi^1_{(++)}$ lies significantly higher than $h_{\text{thr}}$. We denote it $h^1_{(--)}$. Numerically, $h^1_{(--)}=0.336\,837$. Similarly to the third orbit, the solution $\psi^1_{(++)}$ transforms into its ''sister'' complex $\psi^1_{(--)}$. For $h$

TABLE I. The intersoliton separations for the two-soliton collective states. In each of the three cases $z_1$, $z_2$, and $z_3$, the first column is the separation distance for the numerically obtained solution and the second column is its variational approximation. For comparison we also produce the corresponding prediction of the perturbative formula (27) with $k$ given by Eq. (13). In this table $h=0.35$. All calculations were done on the interval $[-100,100]$ using a sixth-order iterative algorithm with the step size $\Delta x=0.025$ and residual value $\delta\sim 10^{-8}$. The exception is marked by an asterisk, where the residual was $\delta=0.5\times 10^{-6}$.

| | $2z_1$ numerical | $2z_1$ variational | $\pi/2k$ | $2z_2$ numerical | $2z_2$ variational | $3\pi/2k$ | $2z_3$ numerical | $2z_3$ variational | $5\pi/2k$ |
|---|---|---|---|---|---|---|---|---|---|
| $\psi_{(++)}$ | 7.60 | 7.95 | 5.120 | | 18.20 | 15.361 | 28.00 | 28.45 | 25.601 |
| $\psi_{(--)}$ | 5.60 | 4.85 | 5.120 | | 15.35 | 15.361 | 26.20 | 25.60 | 25.601 |
| $\psi_{(-+)}$ | | 7.90 | 5.120 | | 17.20 | 15.361 | 28.075* | 27.45 | 25.601 |

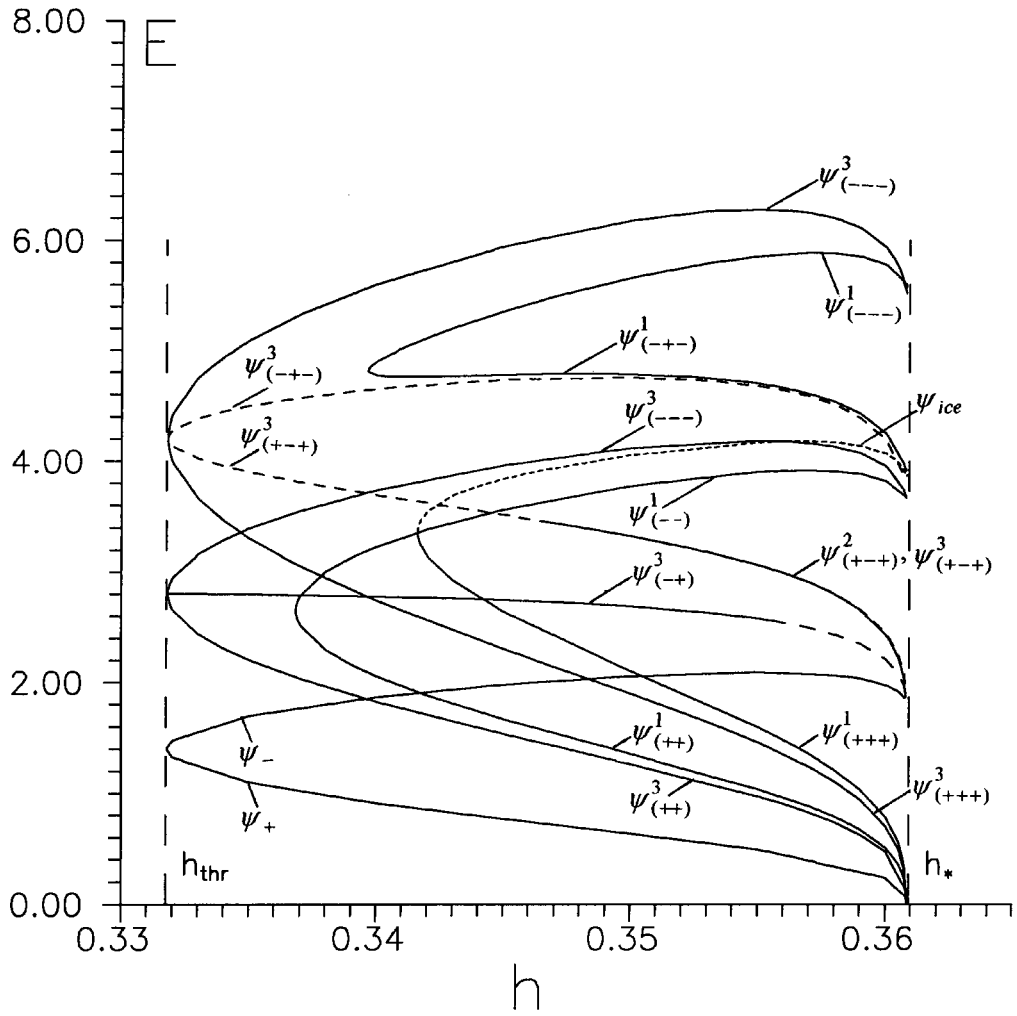


FIG. 5. Bifurcation diagram featuring single-soliton, two-soliton, and symmetric three-soliton solutions. Notice that the branch $\psi^3_{(-+)}$, departing from the triple turning point as a solid line, becomes dashed as it continues to the right. This is meant to indicate that we had to allow for a larger residual of the numerical scheme as we advanced in the direction of larger $h$. We were unable to compute the solution at the dashed part of the curve with the residual $\delta$ smaller than $\sim 10^{-6}$–$10^{-5}$. The branch $\psi^2_{(+-+)}$ (solid curve into which the branch $\psi_-$ turns near the value $h=h_*$) terminates at $h\approx 0.3465$; we were unable to advance it further to the left. This solid curve partially conceals the branch $\psi^3_{(+-+)}$ (second dashed curve from the bottom). The latter starts at about the same point as the curve $\psi^2_{(+-+)}$ but extends all way to the quartic turning point where it turns into the $\psi^3_{(-+-)}$. For those $h$ where the complex $\psi^2_{(+-+)}$ exists, the energies of the two orbits $\psi^2_{(+-+)}$ and $\psi^3_{(+-+)}$ are graphically indistinguishable.

$=0.35$, the variationally predicted and numerically observed separations for this solution are, respectively, $2z_1=4.85$ and $2z_1\approx 5.60$.

Both ''double-$\psi_-$'' complexes are shown in Fig. 7. In the same picture we have also plotted the linear combination $\psi_-\psi_-$ — for exactly the same value of the separation as that of the numerically obtained $\psi^1_{(--)}$ solution.

Finally, we have obtained the *asymmetric* two-soliton solution $\psi^3_{(-+)}$. This complex ''lives'' at the third orbit and detaches from its sister solutions, $\psi^3_{(++)}$ and $\psi^3_{(--)}$ at their merging point $h=h_{\rm thr}=0.331\,806\,5$. At the reference point $h=0.35$, the complex $\psi^3_{(-+)}$ has the orbital distance $2z_3\approx 28.075$, whereas the potential of interaction of the $\psi_+$ and $\psi_-$ solitons has its third maximum at $2z_3=27.45$. The solution in question looks simply like a pair of well-separated solitons $\psi_-$ and $\psi_+$; we are omitting the picture here.

We should mention a computational problem encountered in obtaining this asymmetric solution. For small $h$ close to the turning point we were able to compute it with the numerical residual $\delta\sim 10^{-8}$. However, as we advanced in the direction of greater $h$, the convergence of our numerical algorithm deteriorated and we had to allow for a larger residual. In particular, the portion of the asymmetric branch plotted by the dashed line in Fig. 5 was computed with the residual $\delta\sim 10^{-6}$–$10^{-5}$. The separation value $2z_3=28.075$ in Table I was obtained with the residual $\delta=0.5\times 10^{-6}$. We also have to admit here that we were not able to find the asymmetric solution living on the first (or second) orbit.

### B. Three-soliton complexes

We now proceed to three-soliton associations. Two distinct ''three-$\psi_+$'' solutions detach from the flat background at the point $h=h_*$ (see Fig. 5). One of these corresponds to the first orbit $\psi^1_{(+++)}$ and we will discuss it together with other first-orbit complexes later in this subsection. The second solution [Figs. 8(a) and 8(b)] has the separation $z$

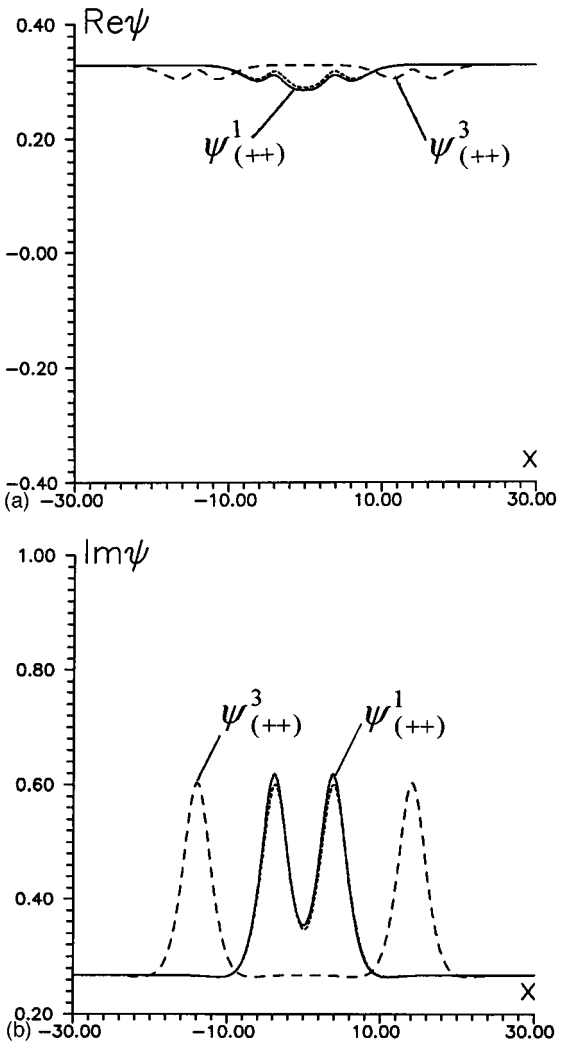


FIG. 6. The two $\psi_{(++)}$ solutions: the first orbit $\psi^1_{(++)}$ (solid line) and the third orbit $\psi^3_{(++)}$ (long-dashed line). For comparison, we also show the linear superposition $\psi_+\psi_+$ for the value of the separation corresponding to $\psi^1_{(++)}$ (short-dashed line).

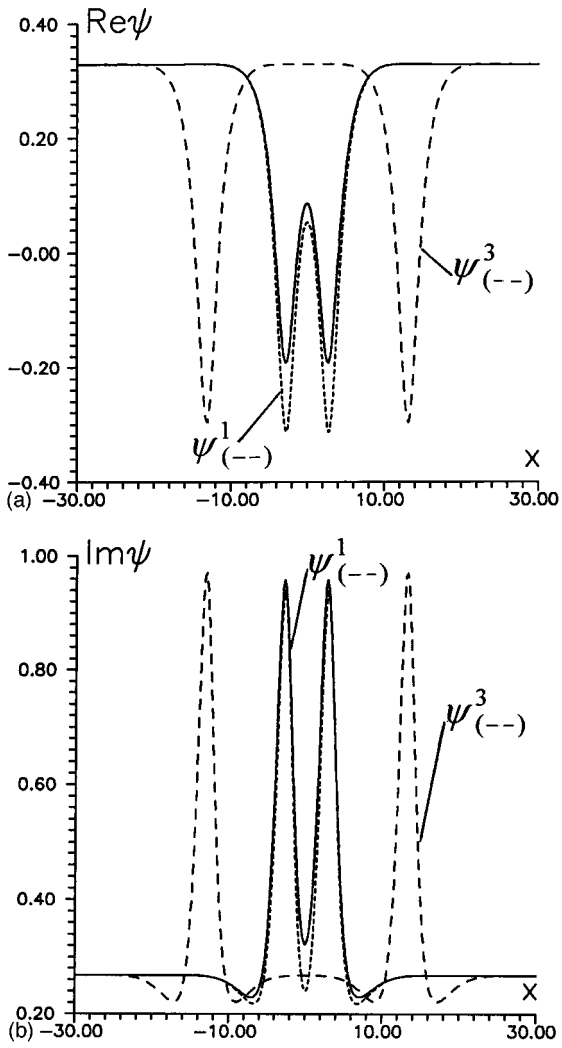


FIG. 7. The two $\psi_{(--)}$ complexes: the first orbit $\psi^1_{(--)}$ (solid line) and the third orbit $\psi^3_{(--)}$ (long-dashed line). The linear superposition $\psi_-\psi_-$ with the same value of the separation as that of $\psi^1_{(--)}$ is also shown for comparison (short-dashed line).

$\approx 28.0$ and, comparing it to the third extremum of $U_{\text{eff}}$ (which lies at $z_3 = 28.425$), we can identify this solution with the third orbit $\psi^3_{(+++)}$.

As $h$ is decreased from $h = h_*$ to the threshold value $h_{\text{thr}} = 0.331\,806\,5$, the third orbit goes over to the $\psi^3_{(---)}$ solution [the uppermost curve in the bifurcation diagram (Fig. 5)]. At $h = 0.35$ the separation distance between the central and the side solitons in this complex is $z_3 \approx 26.175$, which is in a reasonable agreement with the third extremum of $U_{\text{eff}}$: $z_3 = 25.575$. This solution is presented in Figs. 8(c) and 8(d).

We do not plot the linear-superposition approximation to this complex since, due to a very small overlap between constituent solitons, it is indistinguishable from the actual numerical solution. The same applies to all other third-orbit complexes.

At the turning point $h_{\text{thr}} = 0.331\,806\,5$ two more three-soliton branches are tangent to the $\psi^3_{(---)}$-$\psi^3_{(+++)}$ curve. One of these is the $\psi^3_{(+-+)}$ complex, which has $z \approx 25.05$.

TABLE II. Same as Table I, but for the three-soliton collective states.

| | $z_1$ numerical | $z_1$ variational | $\pi/2k$ | $z_2$ numerical | $z_2$ variational | $3\pi/2k$ | $z_3$ numerical | $z_3$ variational | $5\pi/2k$ |
|---|---|---|---|---|---|---|---|---|---|
| $\psi_{(+++)}$ | 7.45 | 7.925 | 5.120 | | 18.175 | 15.361 | 28.00 | 28.425 | 25.601 |
| $\psi_{(---)}$ | 5.95 | 4.70 | 5.120 | | 15.325 | 15.361 | 26.175 | 25.575 | 25.601 |
| $\psi_{(+-+)}$ | 5.02 | 6.925 | 5.120 | 14.80 | 17.275 | 15.361 | 25.05 | 27.50 | 25.601 |
| $\psi_{(-+-)}$ | 8.80 | 7.15 | 5.120 | | 17.275 | 15.361 | 28.75 | 27.50 | 25.601 |

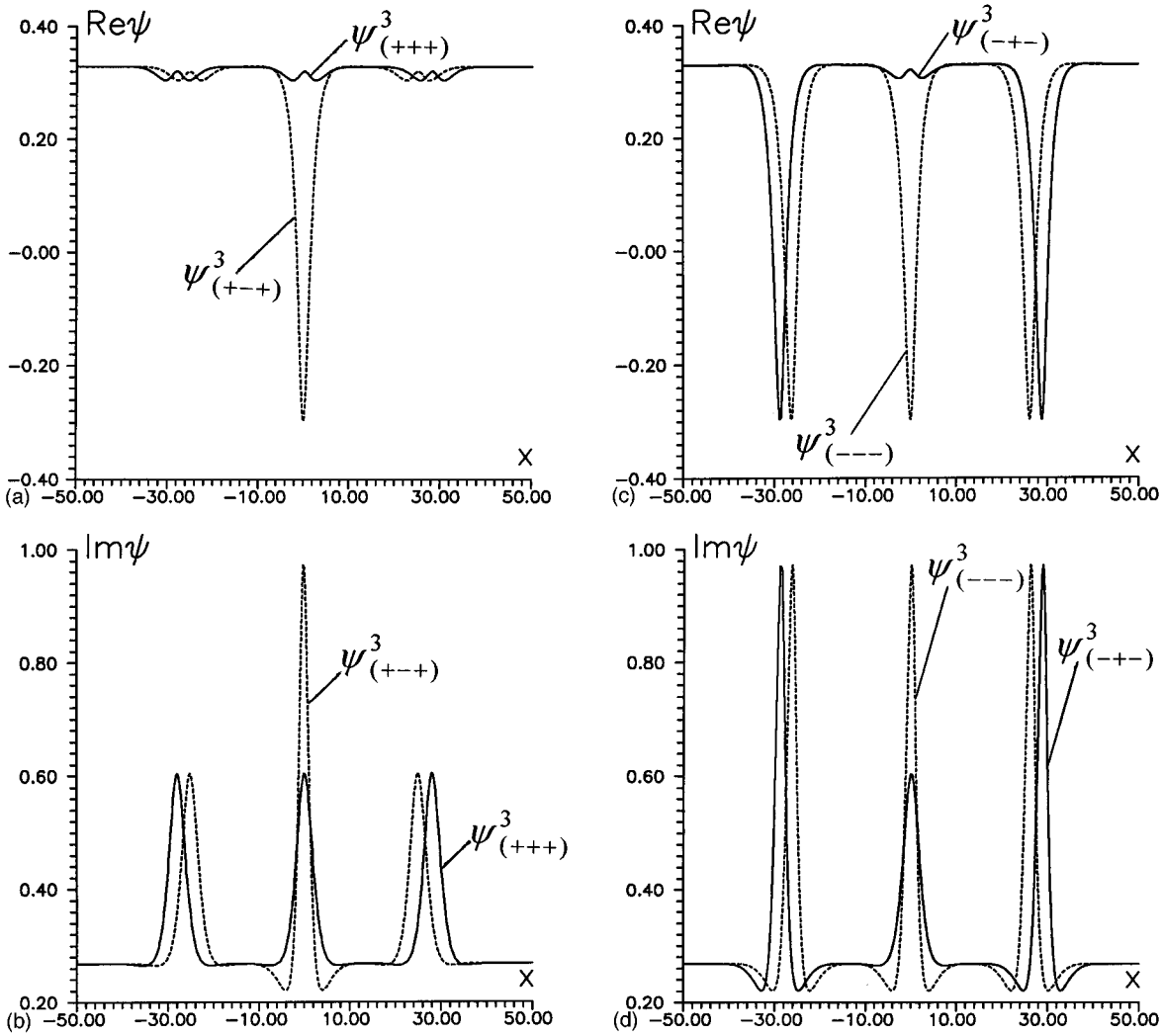


FIG. 8. (a) and (b) $\psi^3_{(+++)}$ (solid line) and $\psi^3_{(+-+)}$ (dashed curve) and (c) and (d) $\psi^3_{(-+-)}$ (solid line) and $\psi^3_{(---)}$ (dashed line). Note that here the solid and short-dashed lines are both used for two pairs of the actual numerical solutions (and not solutions and their linear-superposition approximations as in other figures). Also note the change of the horizontal scale.

The fact that this solution can be identified with the complex $\psi^3_{(+-+)}$ follows from the comparison with the variational estimate, which gives $z_3=27.50$ for the corresponding linear combination, and from the graphical comparison of the two configurations [Figs. 8(a) and 8(b)].

We already encountered a collective state of one $\psi_-$ and two $\psi_+$'s in Sec. II; see Figs. 3(c) and 3(d). However, solitons constituting that complex had the separation distance $z \approx 14.80$, which is close to the *second* extremum of the corresponding interaction potential, $z_2=17.275$. Consequently, the multisoliton solution discussed in Sec. II should be identified with the $\psi^2_{(+-+)}$ complex (i.e., the second orbit).

For those $h$ where the second orbit was found, its energy was practically equal to the energy of the corresponding third orbit $\psi^3_{(+-+)}$ and so the two curves merge into one in Fig. 5. (This is a simple consequence of the fact that the ''binding energy'' of solitons at the second and third orbits is exponentially small due to the very weak overlap and the energy of each complex is not very different from the sum of energies of its constituents.) However, the two orbits differ in their respective domains of existence: We were unable to continue the branch $\psi^2_{(+-+)}$ to the left of the value $h \approx 0.3465$, whereas the complex $\psi^3_{(+-+)}$ exists all the way down to the turning point $h_{\rm thr}=0.331\,806\,5$ (see Fig. 5).

At the turning point $h_{\rm thr}$, the $\psi^3_{(+-+)}$ solution transforms into the $\psi^3_{(-+-)}$ complex. The latter collective state has $z_3 \approx 28.75$, with the variational estimate giving $z_3=27.50$. The corresponding profiles are plotted in Figs. 8(c) and 8(d).

All four three-soliton $\psi^3$ complexes have first-orbit counterparts. We start with the $\psi^1_{(---)}$ branch [Figs. 9(a) and 9(b)], which is the second branch from the top in Fig. 5. The numerically observed multisoliton complex has the intersoliton separation $z_1 \approx 5.95$, while the variational estimate is $z_1=4.70$. At the point $h^1_{(---)}=0.339\,644$ it turns into the $\psi^1_{(-+-)}$ solution, plotted in Figs. 9(c) and 9(d). In this complex, the neighbor solitons sit at the distance $z_1 \approx 8.80$ from one another, while the variational estimate is $z_1=7.15$.

We have already mentioned the $\psi^1_{(+++)}$ branch that detaches from the flat solution [Figs. 9(a) and 9(b)]. The reason why this solution can be identified with the $\psi^1_{(+++)}$ orbit is that it has $z \approx 7.45$, whereas the first maximum of the potential $U_{\rm eff}$ is at $z=7.925$. At the point $h_{\rm ice}=0.341\,612$ it turns into another three-soliton first-orbit complex, which deserves a special comment.

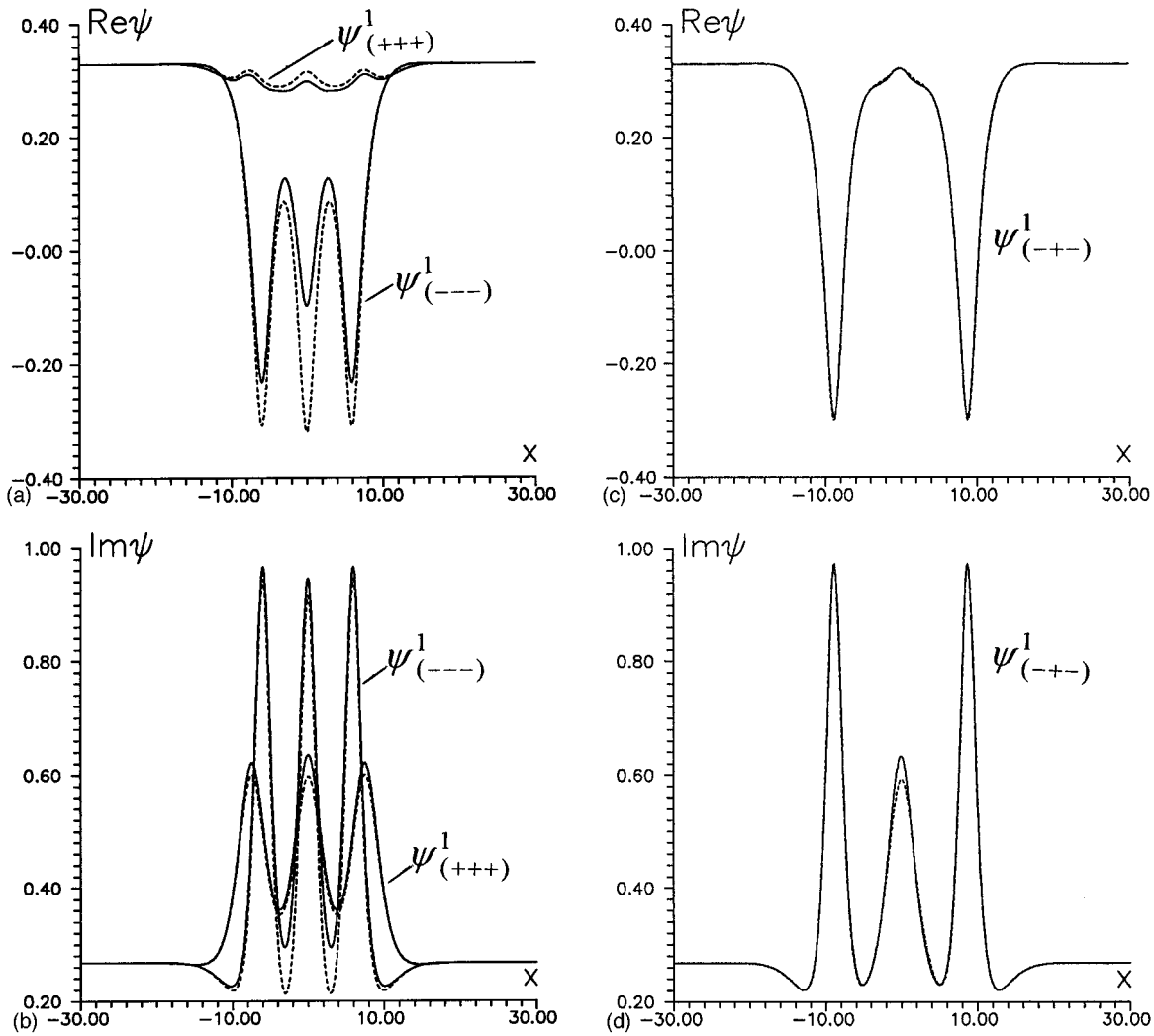


FIG. 9. (a) and (b) $\psi^1_{(+++)}$ and $\psi^1_{(---)}$ complexes (both plotted by solid lines). Short-dashed lines depict their linear-superposition approximations $\psi_+\psi_+\psi_+$ and $\psi_-\psi_-\psi_-$ obtained for the same values of the separation. (c) and (d) $\psi^1_{(-+-)}$ complex (solid line) and its approximation by $\psi_-\psi_+\psi_-$ (dashed line).

The solution in question has a shape similar to an ice-cream cone (Fig. 10). It is not quite obvious whether this solution should be identified with the $\psi^1_{(+-+)}$, $\psi^1_{(---)}$, or some other complex. In an attempt to make an identification, we compare the numerically found ''ice-cream cone'' with the linear combinations $\psi_+\psi_-\psi_+$ [Figs. 10(a) and 10(b)] and $\psi_-\psi_-\psi_-$ [Figs. 10(c) and 10(d)]. Graphically, the $\psi_+\psi_-\psi_+$ seems to provide a better approximation. However, the comparison of energies indicates that the ice-cream cone contains *two* $\psi_-$ constituents. Namely, for large $h$, where the energy of the $\psi_-$ soliton is roughly equal to 2 units and energy of $\psi_+$ is close to zero, the energy of the ice-cream complex is roughly equal to 4. (For comparison, the energies of $\psi^1_{(---)}$ and $\psi^3_{(---)}$ are roughly equal to 6; those of $\psi^3_{(-+-)}$, $\psi^1_{(-+-)}$, $\psi^3_{(--)}$, and $\psi^1_{(--)}$ are in the vicinity of 4 units; and the energies of $\psi^3_{(-+)}$, $\psi^2_{(+-+)}$, and $\psi^3_{(+-+)}$ are near 2.) Thus the question of the composition of the ice-cream complex remains open for the time being.

## V. CONCLUDING REMARKS

A striking feature of the bifurcation diagram (Fig. 5) is almost a total absence of second-orbit complexes predicted by the variational approach. For example, the potential of interaction of two $\psi_-$ solitons has two maxima, at $2z_1 = 4.85$ and $2z_3 = 25.60$, respectively, and a minimum in between, at $2z_2 = 15.35$ (see Table I). However, despite all our attempts, we did not succeed in obtaining the complex $\psi^2_{(--)}$ by means of our Newtonian iterative algorithm. A similar situation occurred for most of the second-orbit complexes; the only exception was the $\psi^2_{(+-+)}$ solution.

A natural question is therefore whether these second orbits are really suppressed by some exclusion principle or this is simply a consequence of a deficiency of our numerical scheme. In order to check on this, we have carried out direct numerical simulations of the full time-dependent NLS equation (2) with the initial condition in the form of the linear combination of two precomputed $\psi_-$ solitons at the distance $2z$ from each other:

$$\psi(x,0) = \psi_-(x+z) + \psi_-(x-z) - \psi_0 . \tag{28}$$

We used a modified split-step pseudospectral method (a generalization of the one described in [14]) with 256 Fourier modes on the interval $-25 \leqslant x \leqslant 25$, with the time increment

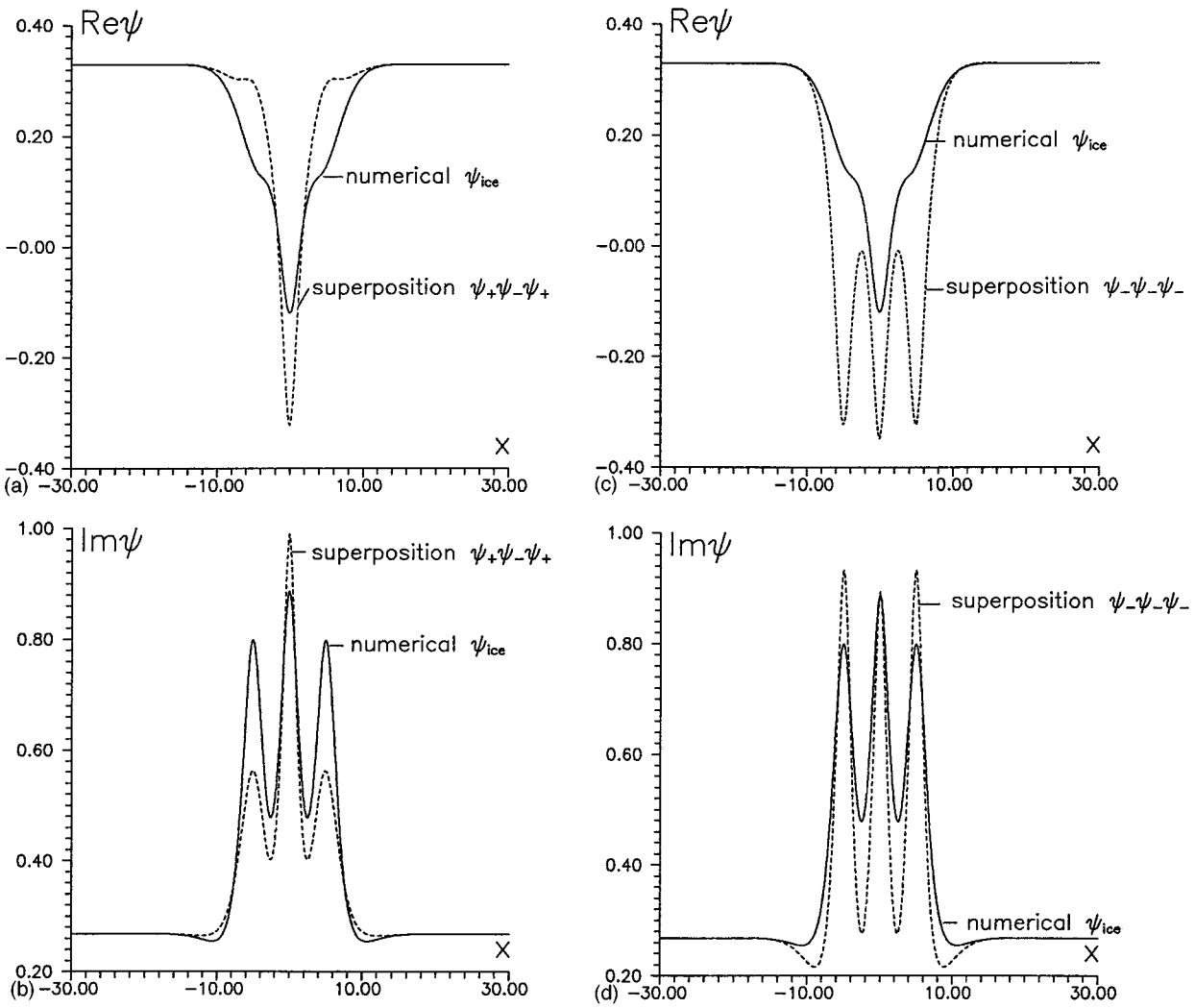


FIG. 10. ''Ice-cream cone'' complex as compared with the (a) and (b) $\psi_+\psi_-\psi_+$ and (c) and (d) $\psi_-\psi_-\psi_-$ linear combinations.

$\Delta t=0.01$. As it was already mentioned, for $h=0.35$ the second extremum of the $U_{\text{eff}}$ is at $z_2=7.7$. Consequently, we have performed two simulations, in the first one setting $z=4$ in the initial condition (28) and in the second one choosing $z=10$. The resulting evolutions are shown in Fig. 11. In both cases solitons moved towards the equilibrium separation $z_2=8.0\pm0.1$ (which is slightly greater than the analytically predicted value 7.7). Since the interaction decays exponentially with distance, the initial separation $z=4$ gives rise to a much faster evolution than the one resulting from $z=10$. In order to eliminate any possible discretization effects, we have repeated the simulations with 512 modes (and the temporal increment $\Delta t=0.0025$) and then with 1024 modes (and $\Delta t=7.5\times10^{-4}$), on the same spatial interval. The results have not been affected, with a more accurate equilibrium soliton separation being $z_2=8.01\pm0.025$.

Thus we conclude that the $\psi^2_{(--)}$ complex does exist for $h=0.35$. (It is appropriate to mention here that the second-orbit two-soliton state had also been observed for stronger dampings, $\gamma=0.6$; see [8].) We still need to understand, however, what prevents us from finding this and other second-orbit complexes within the *stationary* NLS equation (3).

The bifurcation diagram (Fig. 5) is incomplete without understanding of how all multisoliton branches are connected. We have demonstrated numerically that the $\psi_-$ solution continues as the $\psi^2_{(+-+)}$ complex. It is natural to expect more mergers between various pairs (or groups) of branches in a neighborhood of the point $h=h_*$. We speculate that the process of proliferation of soliton complexes always occurs via the ''addition'' of low-energy, small-amplitude $\psi_+$ solitons in the vicinity of the point where $\psi_+$ merges with the background. Details of this mechanism as well as the structure of the bifurcation diagram in the neighborhood of $h=h_*$ are still to be clarified.

Next, when compiling the existence chart for the ac-driven damped NLS solitons, we have identified two characteristic ranges of $\gamma$ values: $\gamma<1/2$ and $\gamma>1/2$ [10]. In the case of $\gamma>1/2$ (which the present paper is devoted to), solitons have oscillatory tails in their entire domain of existence. This gives rise to an oscillatory potential of interaction, whose extrema correspond to stationary collective states of solitons. The fact that the potential $U_{\text{eff}}$ is oscillatory in *an arbitrarily small neighborhood* of the point $h=h_*$ (where the $\psi_+$ soliton merges with the flat solution) is crucial for the mechanism of the formation of solitonic complexes. It allows

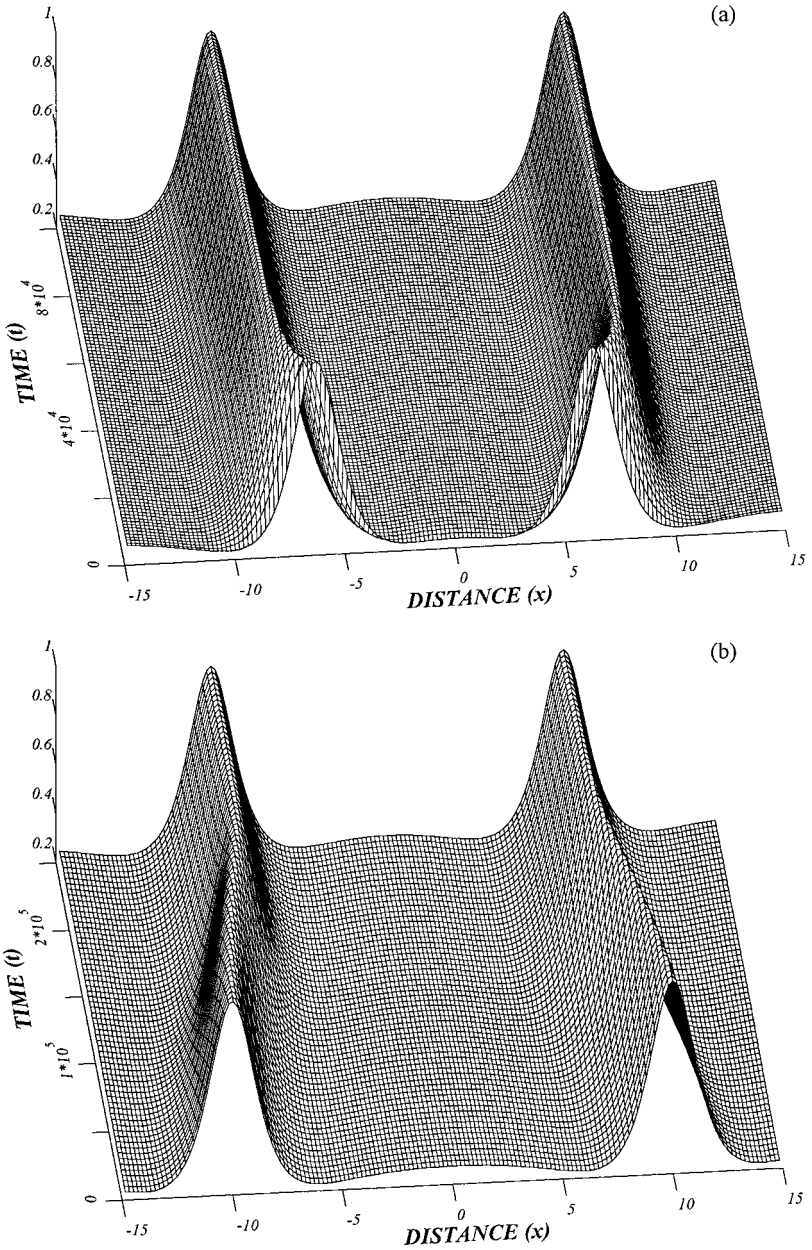


FIG. 11. Evolution of a pair of the $\psi_-$ solitons for the initial separation half distances (a) $z=4$ and (b) $z=10$. Plotted is the imaginary part of $\psi$; the actual $x$ interval $[-25,25]$ has been cut down to $[-15,15]$ for graphical clarity.

the $\psi_+$ solitons to attach to the collective state in the narrow region of $h$ values where their amplitudes and energies are small.

On the other hand, in the case $\gamma<1/2$ neither $\psi_+$ nor $\psi_-$ solitons have oscillatory tails in the vicinity of the merger point, yet multisoliton complexes were observed in computer simulations for $\gamma<1/2$ [9]. It would therefore be interesting to find out what is the mechanism of their proliferation in *that* case. A related open question is on the fate of the $\psi_-$ soliton as $h$ approaches $h_+$, the value for which the soliton's decay exponent vanishes. One possibility could be that the $\psi_-$ soliton turns into a multisoliton branch at some $h<h_+$ (similarly to what we observe in the case $\gamma>1/2$); however, this scenario seems to contradict the fact the potential $U_{\text{eff}}$ is nonoscillatory in the vicinity of $h=h_+$. Alternatively, the $\psi_-$ soliton could exist all way up to the point $h=h_+$, where its type of decay would change to power law. (That is, the $\psi_-$ would approach and finally reach the *algebraic* soliton.) Although it is precisely this second scenario that seems to be supported by the numerical evidence [10], it does not provide any clue on how the multisoliton branch can connect to the rest of the diagram.

Another open question is the multisoliton states' stability and lifetime. The variational two-particle approximation yields a sequence of equilibrium soliton separations, the first one corresponding to a maximum in their interaction potential $U_{\text{eff}}$, the second to a minimum, and so on. Consequently, one could expect that the second orbit will be stable and the first and third orbits unstable (cf. [15]). However, direct numerical simulations do not always support this intuitively

appealing idea. A suitable counterexample comes from the work of Wabnitz [9], who examined the case of $\gamma=0.360$ and $h=0.234$. In this case the soliton's asymptotic value is $|\psi_0|^2=0.061$, the asymptotic wave number $k=0.190$, and the perturbative results (27) for the first two extrema of $U_{\rm eff}$ (the maximum and minimum, respectively) are $2z_1=8.26$ and $2z_2=24.78$. On the other hand, the simulations of Ref. [9] revealed a *stable* stationary soliton doublet with the separation distance $2z\approx 8$. Contrary to what one could have expected from the fact that this bound state is stable, it obviously corresponds to the *maximum* of the interaction potential (i.e., it should be identified with the $\psi^1_{(--)}$ complex).

The fact that some of the multisoliton states may prove to be unstable does not mean they would play no role in the soliton dynamics. Numerical simulations indicate that some *temporally periodic* solitons have a spatial structure similar to the first-orbit two- and three-soliton complexes [16,17] and so the soliton collective states may happen to provide a better starting point for the perturbative or variational construction of time-dependent solutions. Another reason to keep an eye on the unstable states comes from the fact that they will be visited by *chaotic* attractors. Multihump structures were indeed observed in simulations of chaotic regimes in the damped driven sine-Gordon and NLS equations [11,16,17].

It is interesting to compare the soliton separations as predicted by the perturbative formula (27) with positions of the extrema of the potential $U_{\rm eff}$ obtained by the calculation of the energy of two- and three-soliton linear combinations and with the actual separations of solitons in the numerically found multisoliton complexes (that is, to compare the third, second, and first columns in Tables I and II). As it could have been expected, the percentage error in the approximate results decreases as one proceeds from lower to higher orbits and the linear combination approximation becomes more adequate.

There is very good agreement between the perturbative values (27) and positions of extrema of $U_{\rm eff}$ for complexes made up of $\psi_-$ solitons only ($\psi_{(--)}$ and $\psi_{(---)}$). The agreement is worse for complexes involving solitons $\psi_+$. For example, the perturbative value for the third orbit is $5\pi/2k=25.601$, while the full variational results for the $\psi^3_{(---)}$, $\psi^3_{(+-+)}$, and $\psi^3_{(+++)}$ complexes are 25.575, 27.50, and 28.425, respectively. The deterioration of the agreement for complexes involving $\psi_+$ is due to a weaker localization of the $\psi_+$ solitons in the neighborhood of the point $h=h_*$.

Finally, we need to mention that for the collective states of the $\psi_-$ solitons living in the first orbits ($\psi^1_{(--)}$ and $\psi^1_{(---)}$), the perturbative formula (27) gives a somewhat more accurate result than the full variational approach. (See Tables I and II.) The nature of this phenomenon has remained unclear. One possible explanation could be that the relation (27) between the asymptotic wave number and separation distance is deeper than the explicit perturbative expression for the soliton that was used in its derivation.

We mentioned several other computational problems that we faced and that are still awaiting their resolution. These include the continuation of the asymmetric $\psi^3_{(-+)}$ solution in the direction of higher $h$ and the continuation of the $\psi^2_{(+-+)}$ branch towards smaller $h$.

With a single exception of the $\psi^3_{(-+)}$ complex, we did not discuss asymmetric two and three-soliton collective states. We expect asymmetric branches to detach from symmetric complexes at all five turning points. For example, the $\psi^3_{(-++)}$ and $\psi^3_{(--+)}$ solutions should emerge from the quartic turning point, where $\psi^3_{(+++)}$, $\psi^3_{(+-+)}$, $\psi^3_{(-+-)}$, and $\psi^3_{(---)}$ branches converge.

## ACKNOWLEDGMENTS

At various stages of this work we benefited from discussions with M. M. Bogdan, D. E. Pelinovski, and E. V. Zemlyanaya. I.B. and N.A. thank Professor I. V. Puzynin for his hospitality at the Joint Institute for Nuclear Research, Dubna, where this work was completed. Special thanks are due to Professor C. Brink for his support and assistance with research resources. This research was supported by the FRD of South Africa, the University Research Council of the UCT, and the Laboratory for Computing Techniques and Automation of the JINR. The work of Yu.S. was supported by the Russian Foundation for Fundamental Research (Grant No. 97-01-01040).

[1] D. J. Kaup and A. C. Newell, Phys. Rev. B **18**, 5162 (1978).
[2] J. C. Eilbeck, P. S. Lomdahl, and A. C. Newell, Phys. Lett. **87A**, 1 (1981); P. S. Lomdahl, O. H. Soerensen, and P. L. Christiansen, Phys. Rev. B **25**, 5737 (1982); P. S. Lomdahl and M. R. Samuelson, Phys. Rev. A **34**, 664 (1986).
[3] M. M. Bogdan, Ph.D. thesis, Institute of Low Temperature Physics and Engineering, Kharkov, 1980 (unpublished); G. Wysin and A. R. Bishop, J. Magn. Magn. Mater. **54-57**, 1132 (1986); A. M. Kosevich, B. A. Ivanov, and A. S. Kovalev, Phys. Rep. **194**, 118 (1990).
[4] K. Nozaki and N. Bekki, Phys. Rev. Lett. **50**, 1226 (1983); Phys. Lett. **102A**, 383 (1984); J. Phys. Soc. Jpn. **54**, 2363 (1985).
[5] K. Nozaki and N. Bekki, Physica D **21**, 381 (1986).
[6] L. A. Lugiato and R. Lefever, Phys. Rev. Lett. **58**, 2209 (1987); M. Haelterman, S. Trillo, and S. Wabnitz, Opt. Lett. **17**, 745 (1992); Opt. Commun. **91**, 401 (1992).
[7] B. A. Malomed, Phys. Rev. A **44**, 6954 (1991); Phys. Rev. E **47**, 2874 (1993).
[8] D. Cai, A. R. Bishop, N. Grønbech-Jensen, and B. A. Malomed, Phys. Rev. E **49**, 1677 (1994).
[9] S. Wabnitz, Opt. Lett. **18**, 601 (1993).
[10] I. V. Barashenkov and Yu. S. Smirnov, Phys. Rev. E **54**, 5707 (1996).
[11] A. R. Bishop, M. G. Forest, D. W. McLaughlin, and E. A. Overman, Physica D **23**, 293 (1986).
[12] G. Terrones, D. W. McLaughlin, E. A. Overman, and A. J. Pearlstein, SIAM (Soc. Ind. Appl. Math.) J. Appl. Math. **50**, 791 (1990).

[13] I. V. Barashenkov and Yu. S. Smirnov, University of Cape Town Research Report No. RR 3/97, 1997 (unpublished).

[14] J. A. C. Weideman and B. M. Herbst, SIAM (Soc. Ind. Appl. Math.) J. Numer. Anal. **23**, 485 (1986).

[15] A more elaborate perturbation analysis indicates that collective states of $\psi_-$ solitons sitting at the minimum of $U_{\text{eff}}$ can be unstable with respect to *phase* perturbations, but this instability can only set in for extremely small values of $h$. See V. V. Afanasjev, B. A. Malomed, and P. L. Chu, Phys. Rev. E **56**, 6020 (1997).

[16] K. H. Spatschek, H. Pietsch, E. W. Laedke, and Th. Eickermann, in *Singular Behaviour and Nonlinear Dynamics*, edited by T. Bountis and St. Pnevmatikos (World Scientific, Singapore, 1989).

[17] M. Bondila, I. V. Barashenkov, and M. M. Bogdan, Physica D **87**, 314 (1995).